Applied Catalysis B: Environmental 192 (2016) 182–192

Contents lists available at ScienceDirect

Applied Catalysis B: Environmental

journal homepage: www.elsevier.com/locate/apcatb

Iron phthalocyanine-graphene donor-acceptor hybrids for visible-light-assisted degradation of phenol in the presence of H_2O_2

Qinglong Wang[a,b], Haiyan Li[c], Jing-He Yang[d,**], Qian Sun[c], Qiuye Li[a,b], Jianjun Yang[a,b,*]

[a] National & Local Joint Engineering Research Center for Applied Technology of Hybrid Nanomaterials, Henan University, Kaifeng 475004, PR China
[b] Collaborative Innovation Center of Nano Functional Materials and Applications of Henan Province, Henan University, Kaifeng 475004, PR China
[c] College of Chemistry and Chemical Engineering, Henan University, Kaifeng 475004, PR China
[d] Research Center of Heterogeneous Catalysis and Engineering Sciences, School of Chemical Engineering and Energy, Zhengzhou University, Zhengzhou 450001, PR China

ARTICLE INFO

Article history:
Received 15 July 2015
Received in revised form 16 February 2016
Accepted 22 March 2016
Available online 24 March 2016

Keywords:
Iron (II) phthlocyanine
Graphene
Donor-acceptor system
Photocatalytic degradation
Phenol

ABSTRACT

Iron(II) phthalocyanine (FePc) is immobilized on graphene sheets to form a graphene(G)/iron(II) phthalocyanine hybrid (G/FePc) by the π–π stacking method. The resultant hybrids are characterized by UV–vis absorption spectra, FTIR, Raman spectra, BET, TEM, SEM and XRD. The result suggests that the interaction between graphene and FePc follows a donor-acceptor mode and the loading of FePc on graphene sheets not only facilitates the dispersion of FePc on graphene but also promotes the exfoliation of the graphene sheets. These samples are tested for photocatalytic degradation of phenol under visible light irradiation ($\lambda \geq 420$ nm). And the photocatalytic activity of graphene, which is not presented when graphene individually acts on phenol, is greatly enhanced because of the π–π stacking interaction when FePc loaded on graphene. The G/FePc hybrid containing 25 wt.% FePc (G/FePc-0.25) exhibits the best photoactivity among the different loading content of FePc, whose degradation rate for phenol achieves 77.1% in the presence of H_2O_2 under visible light irradiation for 3 h.

1. Introduction

Owing to its importance in solar energy harvesting, photocatalysis and building optoelectronic devices, electron transfer in donor-acceptor assemblies is one of the important studied systems. In the process of nature photosynthesis, the system occurs in the reaction center of photosynthetic porphyrin with rapid charge separation and quantitative quantum yield. Because of this kind of electron transfer, the radical ion pairis spatially and electronically well-isolated, which eliminates the energy wasting [1]. The reorganization energy owning to the well balanced electronic coupling between the electron donor and acceptor entities are the essential to the high charge separation efficiency [2,3]. Several electron donor and acceptor system between porphyrins, phthalocyanines and carbon materials have been studied with the optimizing charge-separation processes [4,5] and these studies imply us the photo- and electro-active units, solvent, donor-acceptor distance are related to the catalytic activity. This means that appropriate interaction between the electron donor and acceptor entities of catalyst can enhance the catalytic effect.

Metallophthalocyanines (MPcs), a two-dimensional structure with 18 π-electron aromatic porphyrin synthetic analogues, are typical photo-sensitizers in a variety of fields due to its excellent semiconductivity and photoconductivity. Dye sensitization has been an efficient and widely applicable method to extend the photo-response region of the wide-band-gap semiconductors among the various explorations for visible-light harvesting. Furthermore, the excellent photochemical properties, thermal stabilities and appropriate redox properties are also to the benefit of them attractive for the sensitization of wide-band-gap semiconductors such as TiO_2 [6–8]. MPcs also render many important biological processes, such as, peroxidase for oxidation, catalase for hydrogen peroxide decomposition, which make them considerable to be used as photocatalysts [9]. The potential of phthalocyanines as homogeneous catalysts has been largely reported, and many soluble substituted phthalocyanines have been synthesized [10–12]. However, the harsh reaction process, uncontrollable products, instability of the structure and different electronic properties from the unsubstituted phthalocyanines have hindered the development

* Corresponding author at: National & Local Joint Engineering Research Center for Applied Technology of Hybrid Nanomaterials, Henan University, Kaifeng 475004, PR China.
** Corresponding author.
E-mail addresses: jhyang@henu.edu.cn (J.-H. Yang), yangjianjun@henu.edu.cn (J. Yang).

http://dx.doi.org/10.1016/j.apcatb.2016.03.047
0926-3373/

of homogeneous catalysts. Thus, they, studied as heterogeneous catalysts, have been dispersed on high surface area carbon substrate [13], encapsulated in zeolites [14,15], and immobilized in mesoporous materials [16–18]. However, the applications of phthalocyanines are hindered by its aggregation, which can be solved by selecting proper support materials.

Graphene (G) has been paid much attention since its first experimental exfoliation in 2004 due to its exceptional electronic and optical properties [19]. With a one-atom-thick sheet of sp^2-hybridized carbon arranged in a honeycomb lattice, graphene is an ideal material due to its two-dimensional geometry, high conductivity and superior electron mobility [20]. Moreover, the conjugated π-electron system of graphene, through π–π stacking, electrostatic interaction and hydrogen bond, has the advantage of preserving the unique electronic properties without serious damage. More importantly, the hybrid combined with the two planar molecules, MPcs and graphene sheet, can be endowed with designed optoelectronic properties. The interaction between phthalocyanine and graphene or graphene oxide through π-π stacking has been widely investigated [21–25]. Moreover, Yang et al. has fabricated cobalt phthalocyanine-graphene complex for electro-catalytic oxidation of dopamine, and it shows significantly improvement in electrochemical performance compared with graphene, CoPc or graphene oxide (GrO), respectively [26]. Mahyari et al. reported a thermally catalyzed aerobic oxidation of alcohols with graphene oxide-iron phthalocyanine, and the result indicates that the primary and secondary alcohols are selectively oxidized into the corresponding aldehydes or ketones under optimal and environmentally-friendly reaction conditions with high conversions [27]. Although there have been many works on degrading phenols or other aromatic compounds using phthalocyanines assisted with H_2O_2 [11,28,29], the MPcs/graphene hybrid through π-π interaction using for degrading pollutants assisted with hydrogen peroxide has rarely been addressed.

Phenol, chlorophenol, and nitrophenol compounds are pollutants of wastewater produced by textile industries, paper-making industries, petrochemical, food-processing industries. High toxicity, recalcitrant to natural degradation, and harmful to environment contribute to their top position of priority control pollutants [30–33]. With the urgent need to relieve the energy crisis, and need for a clean and comfortable environment, photocatalysis becomes one of the most promising and challenging methods for the elimination of pollutants through its efficiency and widely applicability. However, there are two restrictive factors to limit the practical application of photocatalytic degradation of pollutants, that is, the relatively low quantum efficiency and extremely insufficient utilization of solar light. Therefore, many efforts have been made to extend the photo-response region of photocatalyst to visible-light region, such as narrow band-gap semiconductors, composite materials and dye-sensitized semiconductors [34–36].

Herein, we describe the synthesis of non-covalently graphene/iron(II) phthalocyanine hybrid (G/FePc) by a facile method, its characterization, and use for the photocatalytic degradation of phenols with enhanced activity. Because of conjugated π-electron system, phenols can also be adsorbed by G/FePc through π–π interaction [37]. The substrate graphene makes phthalocyanines to be dispersed well and adjusts the electron density of phthalocyanine. So, there is a positive contribution to the higher activity of G/FePc than that of FePc. Comparing to other metal phthalocyanine/graphene been reported previously [38,39], not only do we examine the details of the electron transfer between donor and acceptor, characterized the morphology and structure, but also we employ the G/FePc as catalyst for photocatalytic degradation reaction, we also carefully studied the reaction process and mechanism.

2. Experimental

2.1. Materials and reagents

Iron(II) chloride tetrahdrate and *o*-phthalic anhydride (AR) were purchased from Aladdin. Graphite powder (SP) was purchased from Sinopharm Chemical Reagent Co., Ltd. Unless otherwise stated, other reagents were of analytical grade and used as received.

2.2. Preparation of graphene,FePc, Cs/FePc and Al_2O_3/FePc

The graphene oxide (GO) was synthesized by oxidation of graphite powder according to a modified Hummers' method [40]. Typically, 10 g of graphite powder and equal sodium nitrate were mixed in 230 mL concentrated sulfuric acid under stirring by mechanical agitator in the ice bath, and then 30 g of $KMnO_4$ was slowly added to the mixture within 10 min. After 3 h, the mixture was heated to 308 K for 4 h, and then 460 mL deionized water was added to the mixture drop by drop (<363 K). After that, the temperature of the slurry was kept at 371 K for 3 h. The batch was then poured into a 2 L beaker, the hydrogen peroxide (100 mL, 30%) and hydrochloric acid (300 mL, 37%) were added into the mixture immediately. Remove the supernatant twice a day until Cl^- could not be detected. The mixture was filtered and the cake was put into oven (333 K) for 24 h and then grinded to get GO. And graphene sheets were obtained referring to Li's method [41], 0.4 g of GO was dispersed in 400 mL water by ultrasonic for 30 min and then 4.1 mL of hydrazine hydrate (85%) and 70 mL of ammonia solution were added into the suspension. The solution was kept at 368 K for 3 h. Graphene were obtained by filtration and dried in an air oven at 333 K.

Iron(II) phthalocyanine (FePc) was obtained using low toxic *o*-phthalic anhydride as raw materials by solid-phase synthesis. Typically, *o*-phthalic anhydride, urea, iron(II) chloride tetrahydrate were mixed at a mole ratio of 1:6:0.25, and a small quantity of ammonium molybdate was added as catalyst in the reaction. The mixture was grinded before transferring to the autoclave, which was put into the oven at 453 K for 4 h. The resulting solid was purified by concentrated sulphuric acid (98%), and then added water for recrystal. The precipitate was washed with water until the pH value of the supernatant was neutral. FePc was obtained by vacuum drying for 12 h.

Graphene was selected as the support materials, and multi-wall carbon nanotubes, activated carbon and aluminium oxide were chosen for comparison. The mixture of iron(II) phthalocyanine and carbon materials were added to chloroform under stirring and then ultrasonic treatment for 30 min. The obtained dispersions were filtrated by 0.22 μm filter membrane, and washing the residue with ethanol at least three times and then vacuum drying for 12 h. The preparation method of Al_2O_3/FePc was identical to carbon materials/FePc. The samples were denoted as Cs/FePc-*x*, Cs represents support materials including graphene (G), multi-wall carbon nanotubes (CNTs) and activated carbon (C), *x* was the mass ratio of FePc in hybrid. The amount of the reactants used for preparing the G/FePc-*x* samples described as followed: G/FePc-0.05: FePc 10 mg, G 190 mg; G/FePc-0.15: FePc 30 mg, G 170 mg; G/FePc-0.25: FePc 50 mg, G 150 mg; G/FePc-0.35: FePc 70 mg, G 130 mg; G/FePc-0.45: FePc 90 mg, G 110 mg.

2.3. Characterizations

The Brunauer-Emmett-Teller (BET) surface area (S_{BET}) and the Barrett-Joyner-Halenda (BJH) pore-size distribution of the samples were evaluated on the basis of nitrogen adsorption isotherms measured at 77 K with Quantachrome Quadrasorb SI-4 (USA). Prior to analysis, all samples were degassed at 423 K for 6 h under

vacuum. UV–vis spectrophotometer (UV-2600, SHIMADZU, Japan) was used for collecting the spectroscopic data. X-ray powder diffraction (XRD) patterns were recorded at room temperature by a Bruker D8 Advance X-ray diffractometer (Germany) using Cu $K\alpha$ (λ = 1.5418 nm) radiation, the scan region ranges from 5–80°. Raman spectra were recorded on amicroscopic confocal Raman spectrometer (RM-1000, Renishaw, UK) with an excitation of 633 nm laser light. Fourier transform infrared (FT-IR) spectra were carried out using Bruker VERTEX 70 spectrometer (Germany) with the KBr disc technique. The morphologies of the samples were characterized by transmission electron microscopy (TEM, JEM-2010, JEOL, Japan, accelerating voltage 200 kV) and field emission scanning electron microscope (FE-SEM, Nova NanoSEM 450, FEI, USA).

2.4. Photocatalytic activity test

Phenol solution was selected as assessment system to investigate the photocatalytic activity of graphene/FePc hybrid. A 300W Xe lamp with a 420 nm cut-off glass filter was used as the light source. 100 mL of phenol solution (50 mg/L) was mixed with 20 mg of photocatalyst in a special quartz reactor. The suspensions were ultrasonically treated for 5 min and then magnetically stirring for half an hour in the dark before irradiation to ensure the adsorption/desorption equilibrium (The dark adsorption experiment was conducted for 4 h, as shown in Fig. S1) between photocatalyst powders and phenol, in the meantime, 0.5 mL hydrogen peroxide (30 wt.%, Aladdin) was added to the suspensions. 5 mL of suspensions were sampled every 30 min and centrifuged at 9000 r/min for 10 min to remove the photocatalyst. The filtrates were analyzed by UV–vis spectrophotometer at the detection wavelength of 270 nm. The degradation rate of phenol was calculated by following equation:

$$\eta = \frac{C_0 - C}{C_0} \times 100\% = \frac{A_0 - A}{A_0} \times 100\%$$

where η represented degradation rate of phenol, C_0 and C were initial concentration of phenol solution and concentration of remaining phenol solution, respectively. A_0 was the absorbance of the initial phenol solution before dark absorption, and A was the absorbance of the remaining phenol solution.

Photo-Fenton reaction: 1.8 mg $FeCl_2{\cdot}4H_2O$ was added to 100 mL phenol solution (50 mg/L) under stirring, then adding 0.5 mL hydrogen peroxide to above-mentioned suspensions before irradiation. 5 mL of suspensions were taken from the reaction solution every 30 min, the filtrates were analyzed by UV–vis spectrophotometer.

To confirm the active species in the reaction, ESR was also conducted on a BRUKER(EMX-8/2.7C) spectrometer at ambient temperature. ESR signals of radicals trapped by DMPO (0.02 mol/L), center field 3380 G, sweep width 200 G. The conditions of irradiation and dark state were carried out to investigate the effect of the light on production of hydroxyl radicals. The intermediate analysis was determined by HPLC (Agilent LC-1260, USA). HPLC series is equipped with a reversed-phase C18 column, and the mobile phase for HPLC experiments was a mixture of methanol and water (60:40, v/v). TOC was monitored with a Multi N/C 2100S TOC/TN analyzer. The samples were filtrated with 0.22 μm millipore filter to remove any particles prior to injecting into HPLC and TOC analyzer.

2.5. The calculation of activation energy of H_2O_2 decomposition

Acidic potassium permanganate titration was used to obtain the activation energy of H_2O_2 decomposition. The experimental details were performed according to the followed reaction:

$$2MnO_4^- + 6H^+ + 5H_2O_2 = 2Mn^{2+} + 5O_2\uparrow + 8H_2O$$

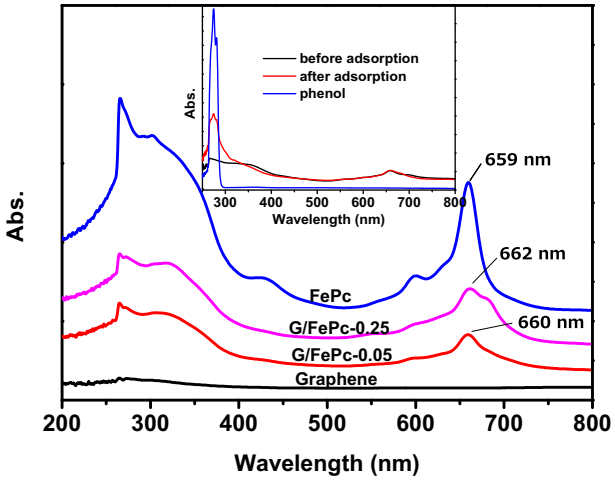

Fig. 1. UV–vis absorption spectra of graphene, G/FePc-0.05, G/FePc-0.25, and FePc in DMF. The inset is the UV–vis absorption spectra of phenol before and after adsorbing on G/FePc-0.25.

$$c(H_2O_2) = \frac{5c(KMnO_4)\Delta V(KMnO_4)}{2V(H_2O_2)} = C \times \Delta V(KMnO_4)$$

C was a constant in the equation. The decomposition of H_2O_2 was considered as a pseudo-first-order with excess solid catalysts.

$$\lg[H_2O_2] = \lg[H_2O_2]_0 - \frac{kt}{2.303}$$

Combined the two above equations, we could get the equation:

$$\lg\Delta V(KMnO_4) = A - \frac{kt}{2.303}$$

where $\Delta V(KMnO_4)$ was volume change of potassium permanganate solution in the reaction, A was a constant, k was apparent rate constant, which could be obtained by the slope of the curve, and t was reaction time. According to Arrhenius equation, we could get the equation as followed:

$$\lg k = -\frac{E_a}{2.303RT} + B$$

where E_a was the activation energy of H_2O_2 decomposition, which could be obtained by the slope of the $\lg k$-$1/T$ curve, R was gas constant, and T was Kelvin temperature.

3. Results and discussion

3.1. Spectroscopic measurements

UV–vis absorption spectra are commonly considered to be an effective technique to characterize the optical properties and identify the chemical structure of the as-prepared materials. UV–vis absorption spectra of graphene, G/FePc and FePc in DMF (*N*, *N*-Dimethyl Formamide) are shown in Fig. 1. The UV–vis absorption of graphene is weak in the whole region of 200–800 nm. FePc shows an increased intensity with characteristic Q-band at 659 nm, which is attributed to the π–π^* transition from the highest occupied molecular orbital (HOMO) to the lowest unoccupied molecular orbital (LUMO) of the FePc molecule [42,43]. An additional weak vibrational satellite band at 600 nm is observed, which is the result of the aggregation between the phthlocyanine units. Compared with FePc, the Q-bands of G/FePc-0.05 and G/FePc-0.25 shift about 1 nm and 3 nm, respectively, indicating that the electronic coupling between the FePc and graphene increases with the proportion of FePc. The

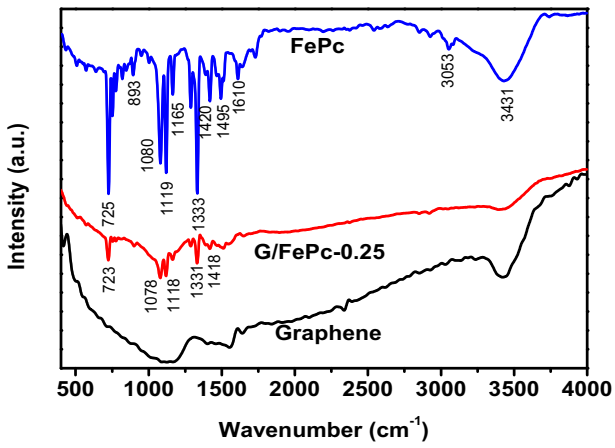

Fig. 2. FTIR spectra of graphene, G/FePc-0.25, and FePc.

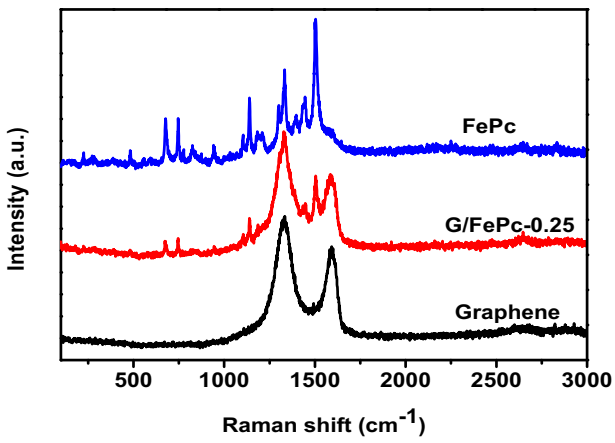

Fig. 3. Raman spectra of graphene, G/FePc-0.25, and pure FePc.

Table 1
IR absorption spectra of FePc and G/FePc-0.25.

FePc (cm^{-1})	G/FePc-0.25 (cm^{-1})	Vibration type
725	723	Vibration of skeleton structure of Pc
1080	1078	
1119	1118	
1165	1161	
1288	1286	C═C stretching vibrations of aromatic nucleus
1333	1331	
1495	–	
1420	1418	C—N stretching vibration
1610	–	C═N stretching vibration
3053	–	N—H vibrations of amide
3431	3420	

disappearance of the peak at 600 nm of the hybrid suggests the well-dispersed FePc on graphene sheet [44]. The inset shows the UV–vis absorption spectra of phenol on G/FePc-0.25 in DMF before and after adsorbing phenol. The hybrid G/FePc-0.25, mixed with the phenol solution under stirring for 4 h in the dark, washed with water and vacuum drying for 12 h, is characterized by UV–vis spectrophotometer. The weak peak at around 660 nm is attributed to the Q band of the photocatalyst, and the strong peak at 274 nm of the phenol in DMF after adsorption for 4 h indicates that the hybrid possesses a good adsorption capacity for phenol.

The vibration of functional groups in the original materials and the hybrid are characterized by FTIR, as shown in Fig. 2 and Table 1. The vibrations of the skeleton structure of phthalocyanine, C═C stretching vibrations of aromatic nucleus, C—N and C═N stretching vibration are listed in Table 1. Besides, the weak peak at 3053 cm^{-1} and the broaden peak at 3431 cm^{-1} are considered as N—H vibrations of amide. The band located at 893 cm^{-1} is related to metal ion, which denotes the formation of metallophthalocyanine due to the coordination between the 3*d* unoccupied orbital of metal atom and nitrogen atom in phthalocyanine ring. It briefly shows in Table 1 that the representative peaks of the G/FePc can be assigned to FePc [44,45]. The slight red shift of all these peaks compared to those of pure FePc indicates a possible π–π stacking formed between graphene and FePc. The shift of the characteristic peaks in C/FePc-0.25, CNTs/FePc-0.25 and Al_2O_3/FePc-0.25 slighter than G/FePc-0.25 or disappeared, as shown in Fig. S2.

The structure of carbon materials can be characterized by Raman spectra (Fig. 3). The Raman spectrum of the G/FePc hybrid shows almost the same signals as those coming from FePc, except for the band at 1504 cm^{-1}, which is assigned to pyrrole C═C stretching mode of FePc [46]. And the spectrum of graphene shows two peaks at 1592 cm^{-1} and 1335 cm^{-1}, corresponding to the G band and D band, which are known to be attributed to in-plane vibration of sp^2-hybridized carbon atoms and defects in the basal plane of graphene, respectively [47,48]. In addition, the two bands appear in the Raman spectrum of the G/FePc hybrid again, confirming the existence of both precursors in the as-prepared hybrid. Moreover, compared with graphene, the G band of G/FePc slightly shifts from 1593 to 1585 cm^{-1}, which can be attributed to the π-π interaction between FePc and graphene [49,50]. However, the G band of C/FePc-0.25, CNTs/FePc-0.25 and Al_2O_3/FePc-0.25 perform no shift compared with graphene, as shown in Fig. S3, which is in accord with FTIR spectra.

3.2. Morphology and microscopic structure analysis

The morphology of the graphene and as-synthesized G/FePc hybrid are characterized by SEM and TEM. Fig. 4(a) shows a typical TEM image of a graphene sheet. The transparent appearance and folded edge with some wrinkles on the sheet is according with the references [51,52]. Compared with graphene sheets, the G/FePc hybrid displays a different morphology (Fig. 4(b)). FePc presents a typical columnar morphology with a length of about 100 nm [53], immobilized on the graphene surface. SEM images shown in Fig. 4(c) and (d) also indicate the same phenomenon. And the morphologies of C/FePc-0.25, CNTs/FePc-0.25 and Al_2O_3/FePc-0.25 are shown in Fig. S4.

The elemental mapping images clearly show the distribution of C and N elements in FePc (Fig. 5(b)) and G/FePc-0.25 (Fig. 5(e)), and both of them are uniformly distributed in the sample particles. Nevertheless, it is unconspicuous in the elemental mapping images due to the very small amount of iron element, however, the existence of Fe can be confirmed by the EDX spectra, as shown in Fig. 5(c, f). All these results clearly indicate the successful synthesis of G/FePc by a facile solid-phase method.

The XRD patterns are used to study the changes in structure of graphene, FePc and G/FePc hybrid. As shown in Fig. 6, the characteristic peaks of graphene are centered at $2\theta = 24.2^\circ$ and 42.8°, corresponding to the (002) and (100) crystal facets, respectively. FePc, tending to aggregate, exhibits a weak reflections at $2\theta = 26.9^\circ$, corresponding to the stacking distance of 0.33 nm between the phthalocyanine moiety within the column [54,55]. The intensity of the characteristic peaks of the G/FePc-0.25 hybrid are lower than that of pristine graphene, which may be attributed to the broadening of (002) inter-planar spacing due to the immobilization of FePc molecules onto graphene. The diffraction peak of G/FePc hybrid at $2\theta = 26.9^\circ$ weakens, indicating that the phenomenon of FePc aggre-

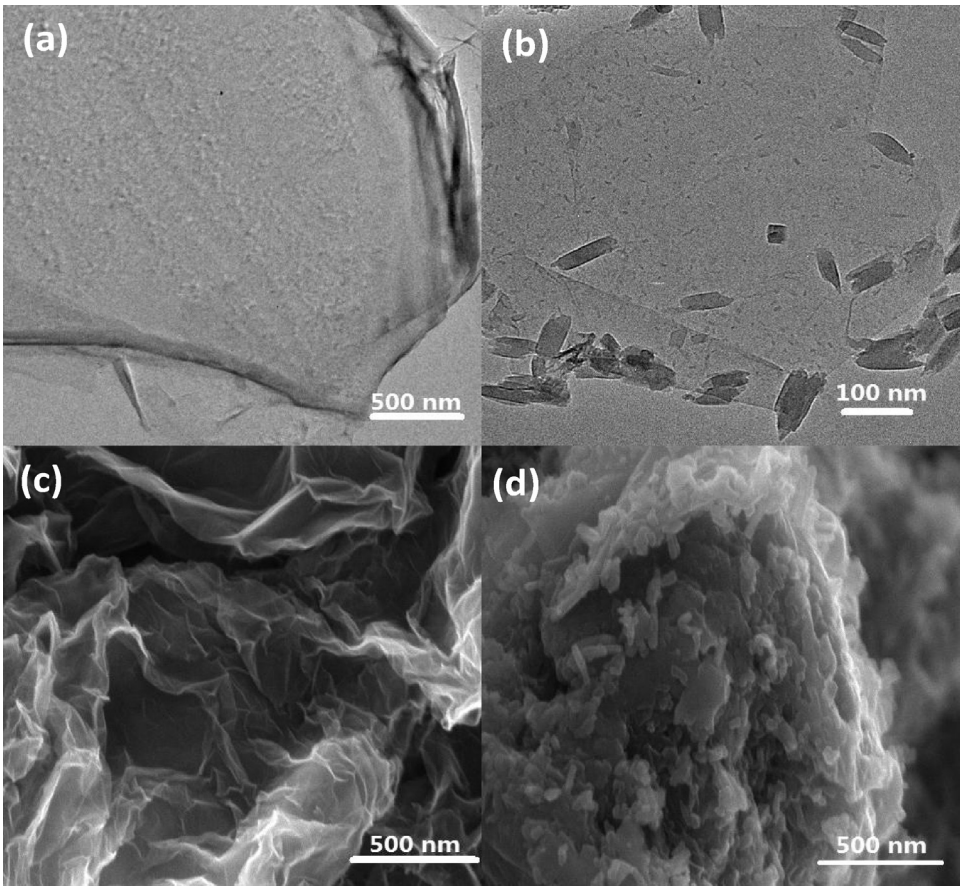

Fig. 4. TEM images of graphene (a) and G/FePc-0.25 (b). SEM images of graphene(c), and G/FePc-0.25 (d).

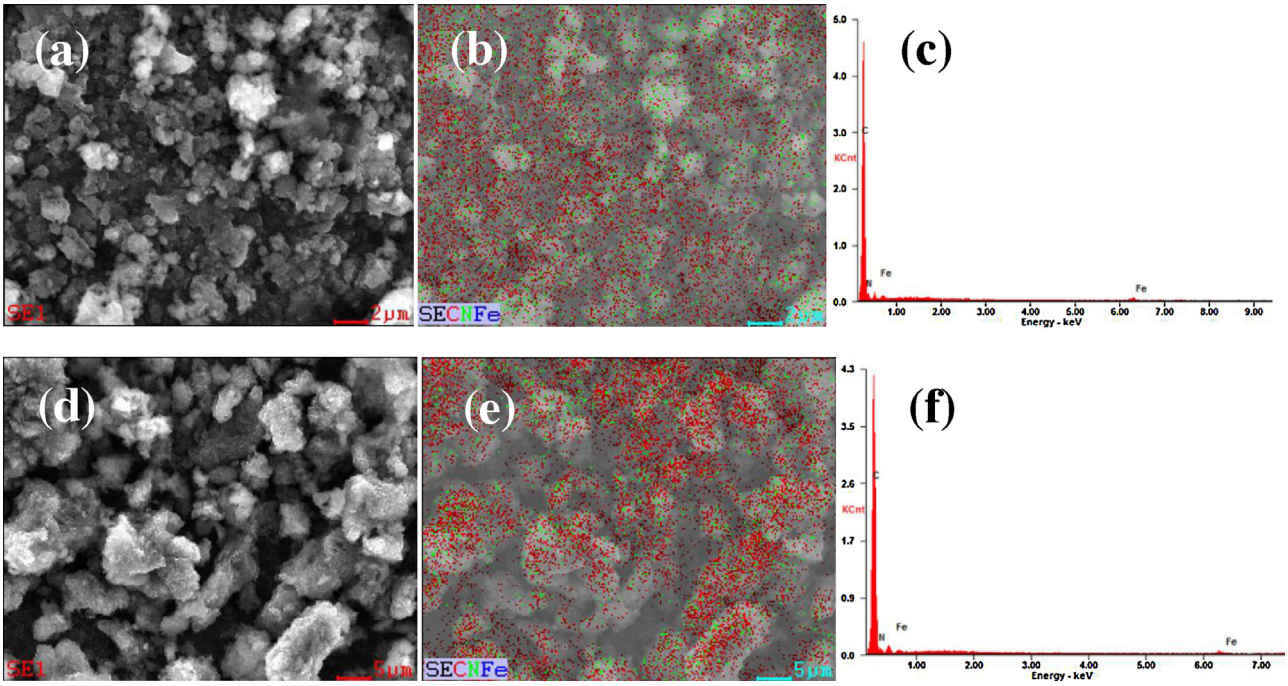

Fig. 5. The elemental mapping images (a), (b) and EDX spectrum (c) of FePc; The elemental mapping images (d), (e) and EDX spectrum (f) of G/FePc-0.25.

gation decreased when dispersing on the graphene sheets. The result is in accordance with that of UV–vis absorption spectra.

The nitrogen adsorption-desorption isotherms are measured to study the specific surface area and BJH pore size distribution of the samples in Fig. 7. The N_2 adsorption-desorption isotherms of

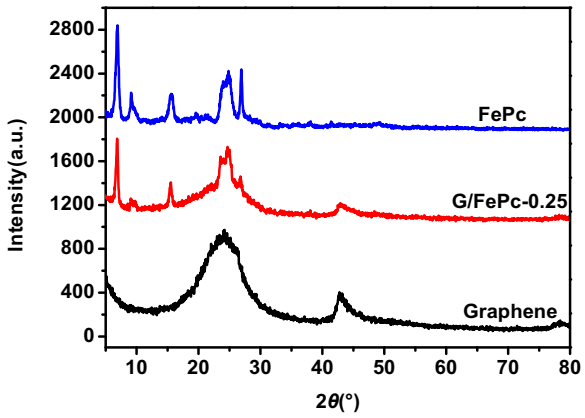

Fig. 6. XRD patterns of graphene, G/FePc-0.25, and FePc.

graphene and G/FePc-0.25 in Fig. 7(a, b) confirm graphene and the hybrid following the type IV with a hysteresis loop of the H3 type corresponding to materials comprised of aggregates (loose assemblages) of plate-like particles forming slit-like pores [56]. The conclusion is also suitable for FePc (Fig. 7(c)). The specific surface area of graphene and the hybrid are as large as 261 m^2/g and 176 m^2/g, respectively, which is beneficial for the adsorption of phenol molecules. Moreover, the two similar curves indicate that the immobilization of FePc onto graphene sheets has no effect on the structure of graphene. Fig. 7(d) shows BJH pore size distribution. Almost all the pore sizes of samples locate at 1.9 nm, corresponding to the layer space between graphene sheets or structural units in FePc nanorod, and another major pore size of FePc at 8.7 nm is also measured, corresponding to the distance of columnar crystals of FePc.

3.3. The calculation of activation energy of hydrogen peroxide

The experimental system is assisted by H_2O_2 to achieve the purpose of efficient oxidative degradation of phenols. The hydroxyl radicals, who are environment-friendly, deriving from the decomposition of H_2O_2, are efficient active species to oxidize pollutants. The mechanism of H_2O_2 decomposition is proposed as followed reactions [57]:

$$H_2O_2 + M \rightarrow 2HO^{\bullet} + M$$

$$HO^{\bullet} + H_2O_2 \rightarrow HO_2^{\bullet} + H_2O$$

$$2HO_2^{\bullet} \rightarrow H_2O_2 + O_2$$

where M represents catalyst. However, there is a difference among the rates of H_2O_2 decomposition in the presence of photocatalysts, due to the different environment and activation energy for H_2O_2. Most of the previous studies have been reported that the catalytic decomposition of H_2O_2 can be considered to be a pseudo-first-order decay kinetics when the solid substance is excess [57,58]. Therefore, the amount of the catalysts is excess in experimental system.

Take FePc for example, Fig. 8(a) shows the relationship between the logarithm of reaction rate constant (lg$k$) and reciprocal of the temperature ($1/T$), and the activation energy of H_2O_2 in the presence of FePc can be obtained according to Arrhenius equation. The reaction rate constant is increasing with the temperature, which is in direct proportion to the rate of H_2O_2 decompo-

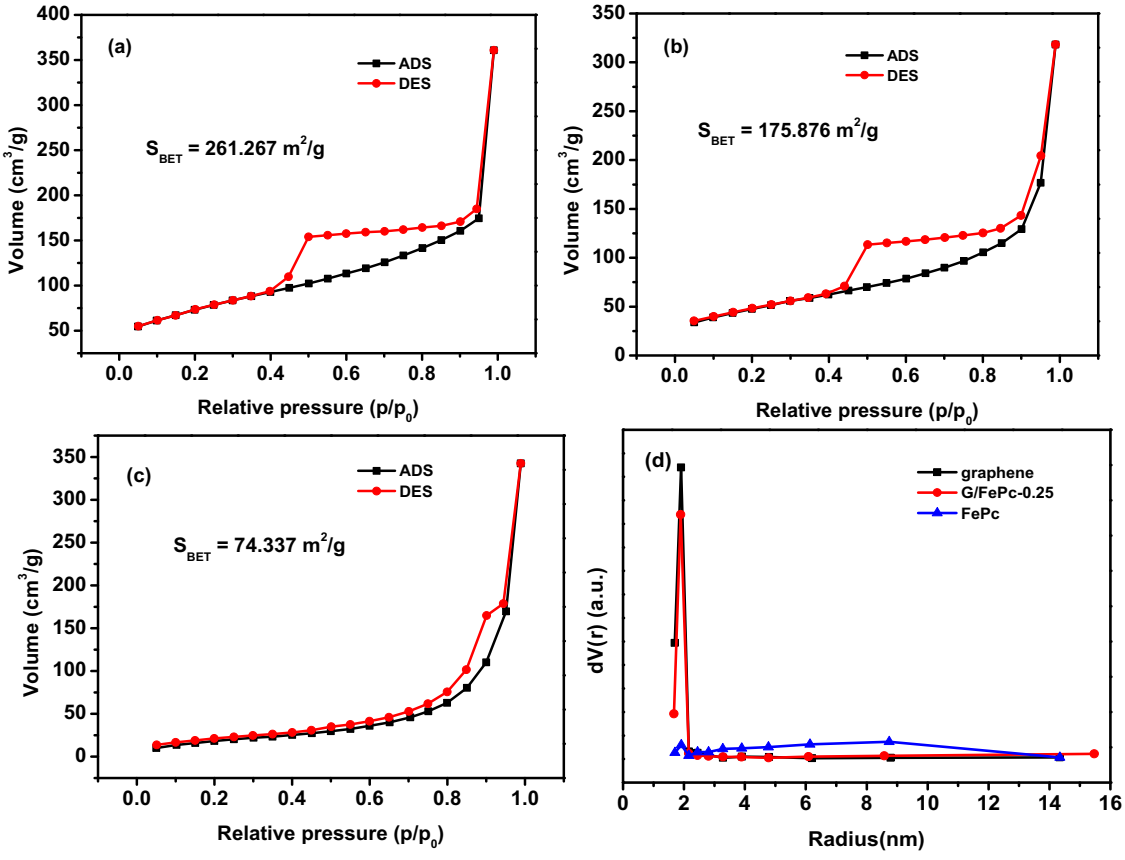

Fig. 7. Nitrogen adsorption-desorption isotherms: (a) graphene; (b) G/FePc-0.25; (c) FePc; (d) BJH pore size distribution.

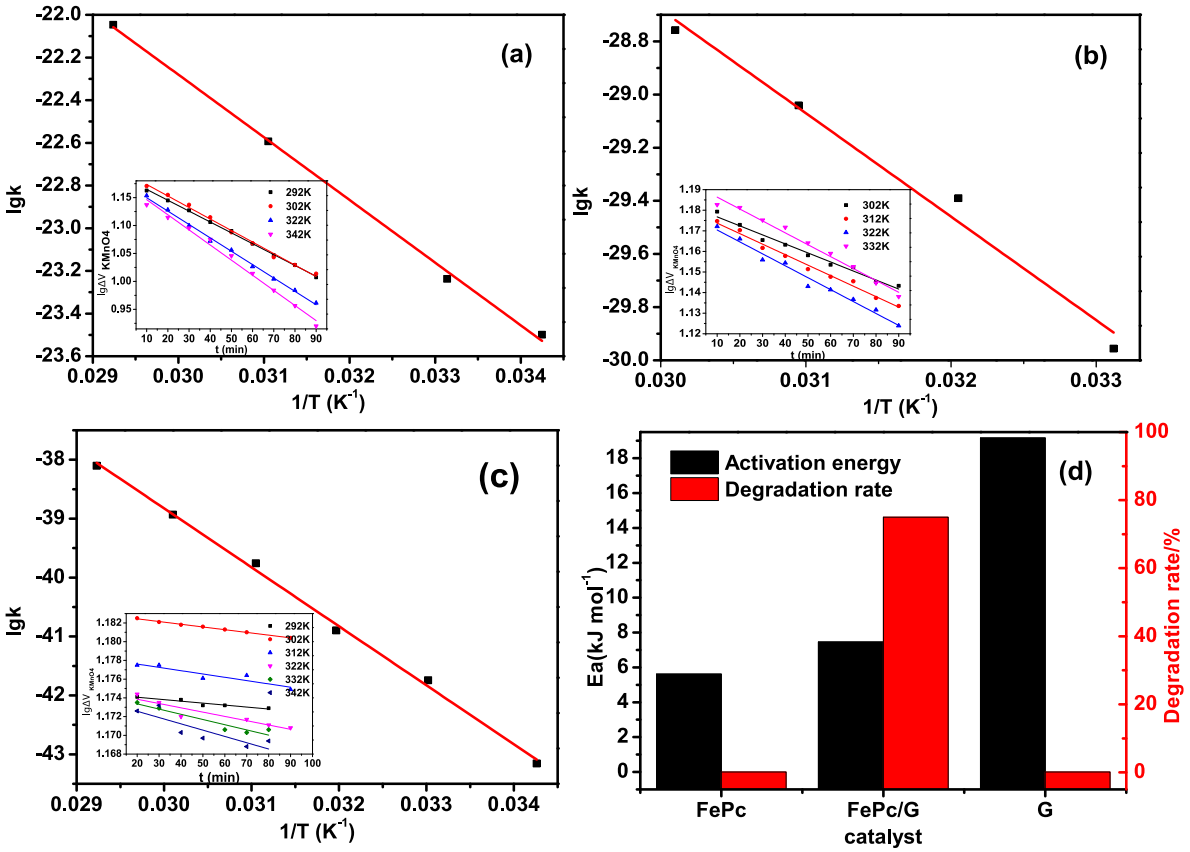

Fig. 8. Arrhenius plots of lg*k* as a function of inverse temperature for FePc (a), G/FePc-0.25(b), and graphene(c). Inset: lgΔV($KMnO_4$) as a function of reaction time for different temperature. Comparison chart of activation energy and degradation rate of phenol (d).

sition. Besides, the inset shows the consumption of potassium permanganate solution within the identical time interval, and the favorable linear indicates the decomposition of H_2O_2 follows first-order kinetics at the certain temperature. The similar explanation can be applied to Fig. 8(b, c). The activation energy (E_a) of H_2O_2 with different catalysts (black column) and the degradation rate of phenol (red column) are shown briefly in Fig. 8(d). As reported in the previous works, phthalocyanines and graphene can be used to simulate the catalyst, especially iron phthalocyanine [9,59], thus reducing the barrier of H_2O_2 decomposition. It is easy to see, E_a(graphene, 19.17 kJ mol^{-1}) > E_a(G/FePc-0.25, 7.46 kJ mol^{-1}) > E_a(FePc, 5.62 kJ mol^{-1}), and only G/FePc performs photocatalytic activity, suggesting that the loading of FePc on graphene sheets decreases the activation energy of H_2O_2, which matches the subsequent adsorption or reaction of phenol and H_2O_2. The active species derived from the H_2O_2 decomposition could not be produced efficiently due to the high activation energy over graphene, on the contrary, the active species could not be fully utilized due to the quick decomposition and thus recombining before reacting with phenol, therefore, the proper decomposition rate of H_2O_2 guarantees sufficient reaction time between hydroxyl radicals and phenol. In summary, it is G/FePc hybrid (electron donor-acceptor system) and appropriate production rate of hydroxyl radicals (dominated by H_2O_2 activation energy over G/FePc hybrid) that contribute to the enhanced photo-activation in degrading phenol.

3.4. Photocatalytic degradation of phenol

The dispersion of FePc can remedy the defection of graphene sheet, therefore, the amount of FePc dispersed on the graphene

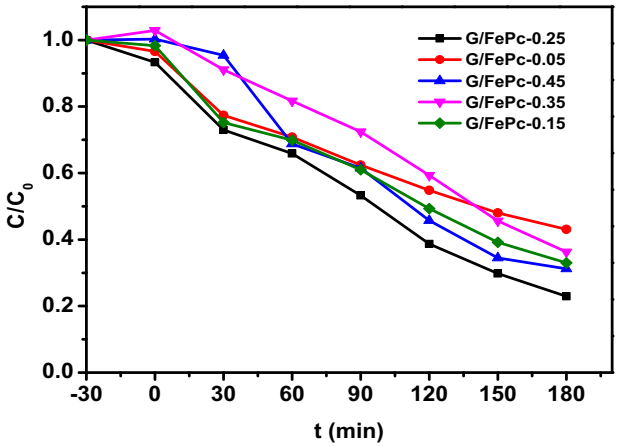

Fig. 9. The optimal experiments: photocatalytic degradation of phenol under visible light ($\lambda \geq 420$ nm) by different FePc fraction of G/FePc.

sheet has effect on the photocatalytic activity of the hybrid. To optimize the content of FePc in G/FePc hybrids, an optimal experiment is carried out in the presence of H_2O_2. As shown in Fig. 9, the percentage of FePc is designed as 5 wt.%, 15 wt.%, 25 wt.%, 35 wt.% and 45 wt.%. The results appeared to be obvious that the ideal photocatalyst is the sample of 25 wt.% of FePc (G/FePc-0.25), the degradation rate of phenol is 77.1% under the visible light irradiation for 3 h. Therefore, the following reactions choose the hybrid of G/FePc-0.25 as the photocatalysts.

Fig. 10(a) shows the degradation of phenol over a series of as-prepared hybrids containing 25 wt.% FePc. All of these photocatalysts rarely perform photocatalytic activity for phenol in the

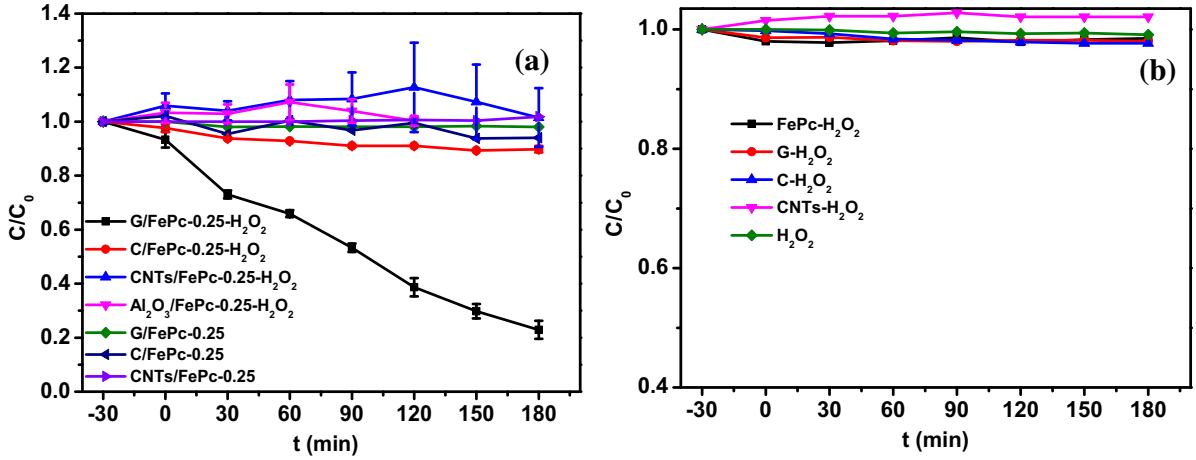

Fig. 10. Photocatalytic degradation of phenol under visible light ($\lambda \geq 420$ nm) by 25 wt.% FePc of different hybrids in the presence/absence of H_2O_2 (a); Photocatalytic degradation of phenol under visible light by individual of FePc and support materials in the presence of H_2O_2 as well as H_2O_2 alone (b).

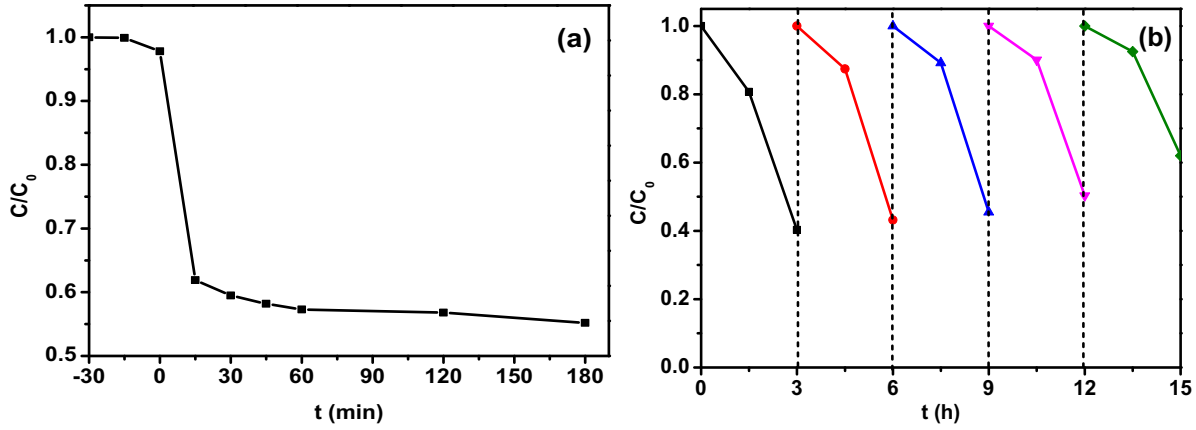

Fig. 11. Fenton reaction (a); cycling experiments of photodegradation of phenol by G/FePc-0.25 (b).

absence of H_2O_2. However, C/FePc-0.25 shows a certain degradation rate (10.2%) in the presence of H_2O_2, and G/FePc-0.25 performs the highest photocatalytic activity, 77.1%, under visible light irradiation for 3 h when the equal hydrogen peroxide is added. Al_2O_3/FePc-0.25 and CNTs/FePc-0.25 are not photoactive to the phenol. That is to say, the equal photocatalysts assisted with equal H_2O_2 display different photocatalytic activity for degrading phenol. Besides, not only hydrogen peroxide alone but also these individual support materials show almost no photocatalytic activity in the presence of H_2O_2, which are shown Fig. 10(b). The above conclusions indicate that the photocatalysts are to assume the leading role in degrading phenol while the hydrogen peroxide is an assisted reagent. And the amount of H_2O_2 has a rather obvious effect on the photocatalytic activity. That is, there is an obvious difference between added 0.25 mL and 0.5 mL of hydrogen dioxide in the reaction system, when the amount of hydrogen dioxide reached to 1 mL, the rate of degradation of phenol just has a slight increment. That is why we choose 0.5 mL of hydrogen dioxide as additive to assist the photocatalytic reaction, as shown in Fig. S5.

Obviously, the introduction of FePc into graphene could significantly enhance the photocatalytic activity, indicating that the π–π stacking interaction between the planar aromatic graphene and FePc serves as a way to transfer electrons from the donor to the acceptor. As is known, Al_2O_3 is a kind of insulating material, thus the electrons injecting from FePc to Al_2O_3 are refused, and the result testifies the mechanism of donor-acceptor mode between support material and FePc. Moreover, the extracts from the suspensions present changes in colors, from colorless to light yellow then to colorless, which implies the formation of benzoquinone during the degradation.

Fenton reaction (Fe^{2+}/H_2O_2), as a homogeneous reaction, produces hydroxyl radicals by interaction of H_2O_2 with ferrous salts:

$$Fe^{2+} + H_2O_2 \rightarrow Fe^{3+} + OH^- + \cdot OH$$

And hydroxyl radicals increase when the system is under irradiation, the mechanism follows equation:

$$Fe^{3+} + H_2O_2 + h\nu \rightarrow Fe^{2+} + \cdot OH + H^+$$

Therefore, the system, containing abundant hydroxyl radicals, exhibits high efficiency for the degradation of organic compounds [60]. To make a comparison with the proceeding work, the photo-Fenton reaction (Fenton reaction assisted with light irradiation) experiment is carried out to make sure whether the photocatalytic reaction in this work is related to Fenton reaction. The result is shown in Fig. 11(a), displaying that the reaction is finished within 15 min after irradiation, and the degradation rate of phenol is lower than G/FePc photocatalyst under visible light irradiation for 3 h. That is to say, the degradation mechanism of phenol, different from the photo-Fenton reaction, is a photocatalytic process dominated by the photocatalyst. Generally, the recycling performance of photocatalyst is significant for its practical application. To investigate the stability of the photocatalyst G/FePc-0.25, the recycle experi-

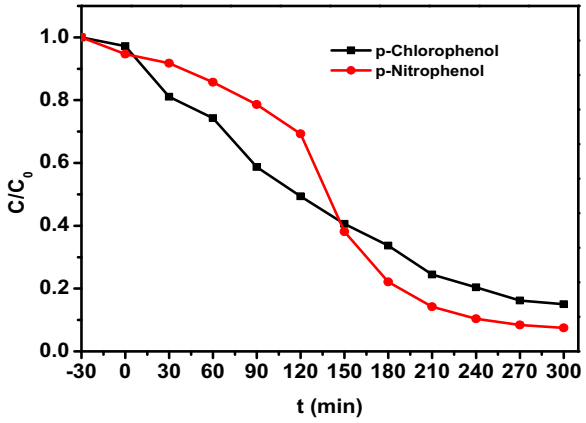

Fig. 12. Photocatalytic degradation of *p*-chlorophenol and *p*-nitrophenol under visible light ($\lambda \geq 420$ nm). Conditions: 20 mg G/FePc-0.25, 100 mL 50 mg/L pollutants, dark condition for 0.5 h, adding 0.5 mL hydrogen peroxide (30 wt.%).

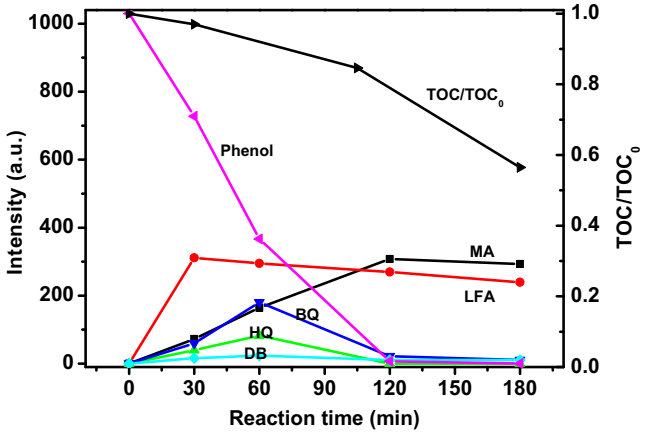

Fig. 13. Distribution of the intermediates and the change of TOC in the photocatalytic degradation of phenol by G/FePc-0.25 under visible light irradiation.

ments are performed, and the results are presented in Fig. 11(b). It is clear that the photocatalytic activity has a limited decline after five recycling experiments. Furthermore, the extend experiments are also carried out to study the universality of the photocatalyst for phenols, thus *p*-chlorophenol and *p*-nitrophenol are selected as pollutants. The results show that both of the pollutants are photodegradable for G/FePc-0.25 (Fig. 12), which indicates that the hybrid is recyclable and promising for future application in environmental technology.

3.5. Analysis of the intermediates and the active species

The common intermediates in the HPLC chromatograms could be confirmed as hydroquinone (HQ), *p*-benzoquinone (BQ), 1, 3-dihydroxybenzene (DB), maleic anhydride (MA) and other low fatty acid (LFA), and the elution order is MA, LFA, HQ, BQ, DB and phenol. Fig. 13 shows that the content of phenol decreases and the intermediates increase, and phenol is almost degraded completely after 2 h, but the C/C_0 value is still high, so it can be called apparent degradation rate of the phenol, the main remaining intermediates are MA and LFA in the reaction system, further oxidation becomes slower and mineralization becomes more difficult, while HQ and BQ are easily oxidized into other intermediates or inorganic carbon. The value of TOC/TOC_0 indicates that the mineralization rate of phenol is only 43.5%, and the degradation rate has reached 77.1% after 3 h.

ESR is used to detect radicals in reaction system. As shown in Fig. 14, there is no ESR signal in the absence of H_2O_2 whether

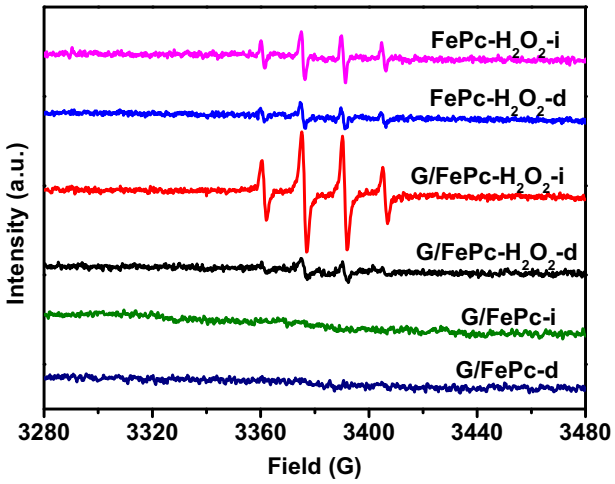

Fig. 14. ESR spectra of the photocatalysts in DMPO solvents in the presence/absence of H_2O_2 under visible light irradiation or dark condition.

under irradiation or dark condition. The characteristic four peaks of DMPO-·OH with intensity of 1:2:2:1 appeared in all system contained H_2O_2 [61], indicating that all of catalysts can decompose hydrogen peroxide with different capacity, which is in accord with the activation energy of hydrogen peroxide. As for the weak intensity of FePc-H_2O_2-i, the reason would be that FePc performs a high capacity to compose H_2O_2 into O_2 quickly, making the amount of hydroxyl radical sharp reduce, so that we can see the bubbles obviously when conducting the experiment. The intensity of peaks in the dark is much lower than that under irradiation, displaying that the light irradiation is to the benefit of the production of ·OH. Moreover, G/FePc-0.25 presents a significant promotion in the intensity of the signal under irradiation compared with individual graphene and FePc, the immobilization of FePc onto graphene is to the benefit of dispersion of FePc, the photo-induced electrons, at a proper generation rate, are transferred to H_2O_2 through π-π stacking, as a result, the hydroxyl radicals are trapped by DMPO efficiently, which is reason for the hybrid performing the optimal photocatalytic activity. Therefore, the conclusion is that the light irradiation and H_2O_2 have a synergistic effect by assisting the photocatalyst on the degradation of phenol.

3.6. The mechanism of the photocatalytic reaction

The π-electron system and large surface area of graphene are determinants to combine FePc by π–π stacking interaction and adsorb phenols with π-conjugated system and H_2O_2. Therefore, a series of reactions occur on the graphene sheet. The mechanism for the photo-degradation of phenol in the presence of FePc photosensitizers is proposed as followed:

$$FePc \xrightarrow{h\nu} FePc^* \rightarrow FePc^+ + e^-$$

$$e^- + H_2O_2 \rightarrow HO\cdot + HO^-$$

$$FePc^+ + H_2O_2 + \text{phenol} \rightarrow FePc + \text{intermediates}$$

$$\text{phenol} \xrightarrow{HO^\bullet} \text{intermediates} \xrightarrow{HO^\bullet} CO_2 + H_2O$$

The schematic diagram of proposed possible mechanism of photocatalytic process is shown in Fig. 15. The π-conjugated district derived from π–π stacking interaction between FePc and graphene acts as the way to transfer electron from the electron donor to the acceptor. FePc with a band gap of about 2.6 eV corresponding to the

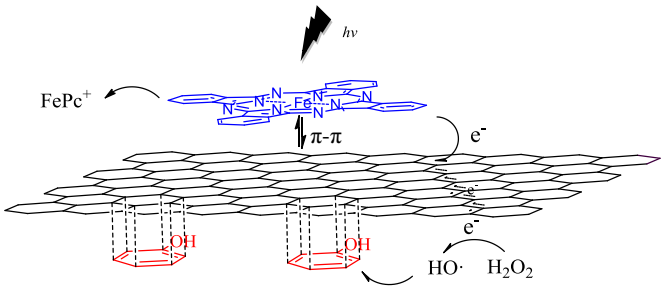

Fig. 15. Schematic diagram of possible mechanism of photocatalytic process.

characteristic absorption of the UV–vis diffuse reflectance spectra at 477 nm turns into excited state ($FePc^*$)under visible light irradiation [62], and $FePc^*$subsequently decomposes into $FePc^+$ and e^-, then, the electron transfers to the graphene sheet via the π-conjugated district and trapped by H_2O_2 to form hydroxide radical, which acts on phenol molecule adsorbed on the graphene sheet and thereby triggering a series of reactions. Besides, FePc can also be recovered from $FePc^+$ in H_2O_2-phenol system, harvesting visible light to keep the reaction continuous.

4. Conclusions

In summary, a hybrid containing FePc and graphene through π-π interaction is synthesized by a simple, facile and cost-effective method. The as-prepared G/FePc photocatalyst possesses considerable photocatalytic activity for degradation of unmanageable phenols. The enhanced photocatalytic performance of G/FePc could be attributed to the perfect dispersibility of FePc on graphene sheets, which provide more active sites and the facilitated electron transfer by the graphene support. Compared with other Cs/FePc and Al_2O_3/FePc samples, G/FePc performs the highest degradation rate assisted by hydrogen peroxide under visible light irradiation for 3 h, and G/FePc-0.25 is the optimal photocatalyst among the different ratio of FePc, whose degradation rate for phenol achieves 77.1% in the presence of H_2O_2 under visible light irradiation for 3 h, while other photocatalysts show the low degradation activity. However, there is no photocatalytic activity in the absence of H_2O_2 in the reaction system, indicating that H_2O_2 acts as an electron acceptor transferring from the FePc-graphene hybrid, and H_2O_2 is the generator of hydroxyl radical, which is the major active species in degrading phenols. Moreover, compared with graphene and FePc, the as-synthesized G/FePc has a proper catalytic capacity to decompose H_2O_2 into hydroxyl radical.

Author contributions

The manuscript was written through contributions of all authors. Q.L. Wang and H.Y. Li contributed equally. J.J. Yang and J.H. Yang decided the manuscript final version. All authors read and approved the final manuscript.

Acknowledgements

The authors gratefully acknowledge the support of the National Natural Science Foundation of China (grant Nos. 20973054, 21403053, U1404503, Nos. 21103042 and 21471047), Program for Science & Technology Innovation Talents (15HASTIT043) and Innovative Research Team (16IRTSTHN015) from the University of Henan Province, and Program for Changjiang Scholars and Innovative Research Team in University from the Ministry of Education of China (PCS IRT1126).

Appendix A. Supplementary data

Supplementary data associated with this article can be found, in the online version, at http://dx.doi.org/10.1016/j.apcatb.2016.03.047.

References

[1] P. Jordan, P. Fromme, H.T. Witt, O. Klukas, W. Saenger, N. Krauss, Nature 411 (2001) 909–917.
[2] H. Imahori, S. Fukuzumi, Adv. Funct. Mater. 14 (2004) 525–536.
[3] H.M. Feier, O.G. Reid, N.A. Pace, J. Park, J.J. Bergkamp, A. Sellinger, D. Gust, G. Rumbles, Adv. Energy Mater. (2016).
[4] D.M. Guldi, G.M. Rahman, F. Zerbetto, M. Prato, Acc. Chem. Res. 38 (2005) 871–878.
[5] Y. Kawashima, K. Ohkubo, V.M. Blas-Ferrando, H. Sakai, E. Font-Sanchis, J. Ortiz, F. Fernandez-Lazaro, T. Hasobe, A. Sastre-Santos, S. Fukuzumi, J. Phys. Chem. B 119 (2015) 7690–7697.
[6] L. Giribabu, V.K. Singh, C.V. Kumar, Y. Soujanya, P.Y. Reddy, M.L. Kantam, Sol. Energy 85 (2011) 1204–1212.
[7] Z. Guo, B. Chen, J. Mu, M. Zhang, P. Zhang, Z. Zhang, J. Wang, X. Zhang, Y. Sun, C. Shao, Y. Liu, J. Hazard. Mater. 219–220 (2012) 156–163.
[8] R.S. Jack, G.A. Ayoko, M.O. Adebajo, R.L. Frost, Environ. Sci. Pollut. Res. Int. 22 (2015) 7439–7449.
[9] H.J. Mackintosh, P.M. Budd, N.B. McKeown, J. Mater. Chem. 18 (2008) 573–578.
[10] J. Gong, D. Li, J. Huang, L. Ding, Y. Tong, K. Li, C. Zhang, Catal. Lett. 144 (2013) 487–497.
[11] C. Colomban, E.V. Kudrik, P. Afanasiev, A.B. Sorokin, Catal. Today 235 (2014) 14–19.
[12] T.B. Ogunbayo, T. Nyokong, J. Mol. Catal. A: Chem. 350 (2011) 49–55.
[13] G. Bottari, G. de la Torre, T. Torres, Acc. Chem. Res. 48 (2015) 900–910.
[14] R.M. Mohamed, M.M. Mohamed, Appl. Catal. A: Gen. 340 (2008) 16–24.
[15] N. Ohata, Y. Ito, D. Nakane, H. Kitamura, H. Masuda, J. Porphyrins Phthalocyanines 19 (2015) 372–376.
[16] M. Silva, M.J. Calvete, N.P. Goncalves, H.D. Burrows, M. Sarakha, A. Fernandes, M.F. Ribeiro, M.E. Azenha, M.M. Pereira, J. Hazard. Mater. 233–234 (2012) 79–88.
[17] S.V. Sirotin, A.Y. Tolbin, I.F. Moskovskaya, S.S. Abramchuk, L.G. Tomilova, B.V. Romanovsky, J. Mol. Catal. A: Chem. 319 (2010) 39–45.
[18] N.C. López Zeballos, M.C. García Vior, J. Awruch, L.E. Dicelio, Dyes Pigm. 113 (2015) 145–150.
[19] K.S. Novoselov, A.K. Geim, S.V. Morozov, D. Jiang, Y. Zhang, S.V. Dubonos, I.V. Grigorieva, A.A. Firsov, Science 306 (2004) 666–669.
[20] Q. Xiang, J. Yu, M. Jaroniec, Chem. Soc. Rev. 41 (2012) 782–796.
[21] A. Chunder, T. Pal, S.I. Khondaker, L. Zhai, J. Phys. Chem. C 114 (2010) 15129–15135.
[22] G.I. Caírdenas-Jiroín, P. Leon-Plata, D. Cortes-Arriagada, J.M. Seminario, J. Phys. Chem. C 115 (2011) 16052–16062.
[23] J.-H. Yang, Y. Gao, W. Zhang, P. Tang, J. Tan, A.-H. Lu, D. Ma, J. Phys. Chem. C 117 (2013) 3785–3788.
[24] G.I. Cárdenas-Jirón, P. León-Plata, D. Cortes-Arriagada, J.M. Seminario, J. Phys. Chem. C 117 (2013) 23664–23675.
[25] O. Taratula, M. Patel, C. Schumann, M.A. Naleway, A.J. Pang, H. He, O. Taratula, Int. J. Nanomed. 10 (2015) 2347–2362.
[26] J. Yang, D. Mu, Y. Gao, J. Tan, A. Lu, D. Ma, J. Nat. Gas Chem. 21 (2012) 265–269.
[27] M. Mahyari, A. Shaabani, Appl. Catal. A: Gen. 469 (2014) 524–531.
[28] O.V. Zalomaeva, A.B. Sorokin, New J. Chem. 30 (2006) 1768.
[29] A.B. Sorokin, E.V. Kudrik, Catal. Today 159 (2011) 37–46.
[30] D. Li, S. Ge, J. Huang, J. Gong, P. Yan, W. Lu, G. Tiana, L. Ding, Catal. Commun. 45 (2014) 95–99.
[31] Y. Yao, Z. Yang, H. Sun, S. Wang, Ind. Eng. Chem. Res. 51 (2012) 14958–14965.
[32] S. Yang, J.-S. Gu, H.-Y. Yu, J. Zhou, S.-F. Li, X.-M. Wu, L. Wang, Sep. Purif. Technol. 83 (2011) 157–165.
[33] M. Ghodrati, M. Haghighi, J. Soltan Mohamdzadeh, B. Pourabas, E. Pipelzadeh, React. Kinet. Mech. Catal. 104 (2011) 49–60.
[34] G. An, W. Ma, Z. Sun, Z. Liu, B. Han, S. Miao, Z. Miao, K. Ding, Carbon 45 (2007) 1795–1801.
[35] Z. Zhang, W. Wang, D. Jiang, J. Xu, Catal. Commun. 55 (2014) 15–18.
[36] Q. Sun, Y. Xu, J. Phys. Chem. C 113 (2009) 12387–12394.
[37] X. Zhao, Y. Li, J. Wang, Z. Ouyang, J. Li, G. Wei, Z. Su, ACS Appl. Mater. Interfaces 6 (2014) 4254–4263.
[38] B.-P. Jiang, L.-F. Hu, D.-J. Wang, S.-C. Ji, X.-C. Shen, H. Liang, J. Mater. Chem. B 2 (2014) 7141–7148.
[39] P. Kumar, A. Kumar, B. Sreedhar, B. Sain, S.S. Ray, S.L. Jain, Chemistry 20 (2014) 6154–6161.
[40] W.S. Hummers Jr., R.E. Offeman, J. Am. Chem. Soc. 80 (1958) 1339.
[41] D. Li, M.B. Muller, S. Gilje, R.B. Kaner, G.G. Wallace, Nat. Nanotechnol. 3 (2008) 101–105.
[42] A.E.H. Machado, M.D. França, V. Velani, G.A. Magnino, H.M.M. Velani, F.S. Freitas, P.S. Müller, C. Sattler, M. Schmücker, Int. J. Photoenergy 2008 (2008) 1–12.

[43] G. Palmisano, M.C. Gutierrez, M.L. Ferrer, M.D. Gil-Luna, V. Augugliaro, S. Yurdakal, M. Pagliaro, J. Phys. Chem. C 112 (2008) 2667–2670.
[44] J.P. Mensing, T. Kerdcharoen, C. Sriprachuabwong, A. Wisitsoraat, D. Phokharatkul, T. Lomas, A. Tuantranont, J. Mater. Chem. 22 (2012) 17094.
[45] C. Zhang, R. Hao, H. Yin, F. Liu, Y. Hou, Nanoscale 4 (2012) 7326–7329.
[46] P. Kumar, G. Singh, D. Tripathi, S.L. Jain, RSC Adv. 4 (2014) 50331–50337.
[47] S.P. Lonkar, Y.S. Deshmukh, A.A. Abdala, Nano Res. (2014).
[48] Y. Jiang, Y. Lu, X. Lv, D. Han, Q. Zhang, L. Niu, W. Chen, ACS Catal. 3 (2013) 1263–1271.
[49] B. Das, R. Voggu, C.S. Rout, C.N. Rao, Chem. Commun. (2008) 5155–5157.
[50] J. Geng, H.-T. Jung, J. Phys. Chem. C 114 (2010) 8227–8234.
[51] C.N. Rao, A.K. Sood, K.S. Subrahmanyam, A. Govindaraj, Angew. Chem. 48 (2009) 7752–7777.
[52] V.H. Pham, T.V. Cuong, S.H. Hur, E. Oh, E.J. Kim, E.W. Shin, J.S. Chung, J. Mater. Chem. 21 (2011) 3371–3377.
[53] J.A.A.W. Elemans, R. van Hameren, R.J.M. Nolte, A.E. Rowan, Adv. Mater. 18 (2006) 1251–1266.
[54] M. Kimura, T. Muto, H. Takimoto, K. Wada, K. Ohta, K. Hanabusa, H. Shirai, N. Kobayashi, Langmuir 16 (2000) 2078–2082.
[55] M. Kimura, K. Wada, K. Ohta, K. Hanabusa, H. Shirai, N. Kobayashi, J. Am. Chem. Soc. 123 (2001) 2438–2439.
[56] M. Kruk, M. Jaroniec, Chem. Mater. 13 (2001) 3169–3183.
[57] C.u.M. Lousada, M. Jonsson, J. Phys. Chem. C 114 (2010) 11202–11208.
[58] S.-S. Lin, M.D. Gurol, Environ. Sci. Technol. 32 (1998) 1417–1423.
[59] J.-H. Yang, G. Sun, Y. Gao, H. Zhao, P. Tang, J. Tan, A.-H. Lu, D. Ma, Energy Environ. Sci. 6 (2013) 793.
[60] M. Cheng, W. Ma, J. Li, Y. Huang, J. Zhao, Y.x. Wen, Y. Xu, Environ. Sci. Technol. 38 (2004) 1569–1575.
[61] Y. Liu, Y. Zhu, J. Xu, X. Bai, R. Zong, Y. Zhu, Appl. Catal. B: Environ. 142–143 (2013) 561–567.
[62] G.D. Sharma, R. Kumar, M.S. Roy, Sol. Energy Mater. Sol. Cells 90 (2006) 32–45.